$Cu_2O/ZnFe_2O_4$ nanorod photoelectrode for photoelectrochemical water splitting

T. Singha, T. Kansa-ard, S. Wannapop, A. Somdee*
Faculty of Science, Energy, and Environment, King Mongkut's University of Technology North Bangkok, Rayong Campus, Rayong 21120, Thailand

Photoelectrochemical water splitting is a promising technology for H_2 generation via water splitting reaction using the semiconductor material. In this research, the $ZnFe_2O_4/Cu_2O$ nanorod was investigated. The products were synthesized by the electrochemical deposition method. The characteristics of materials were investigated by X-ray diffraction, scanning electron microscopy, and UV-visible spectroscopy. All materials exhibited the p-type photoelectrode characteristic. The performance of photoelectrochemical electrodes was studied by linear swept voltammetry, electrochemical impedance spectroscopy, and Mott-Schottky analysis. The best condition deposition was by applying -0.4 V and 10 min. The highest photocurrent density was 0.8 $mA.cm^{-2}$ at -0.5 (vs. Ag/AgCl) bias voltage.

(Received April 7, 2024; Accepted June 17, 2024)

Keywords: Photoelectrochemical cell, Photocathode, Hydrogen energy, $ZnFe_2O_4$, Heterostructure

1. Introduction

Hydrogen (H_2) is an abandon earth element that is much importance for our utilized in daily day life [1]. In particular, the use of H_2 for energy has become a topic development and application in many field of energy conversion and storage. Since, H_2 can be product in many processes [2-4], e.g. steam methane reforming process [5,6] and electrolysis process [7,8]. The steam reforming process is commonly used to product the H_2 for many industries. However, according to the reduction that is emitted the CO_2, the steam reforming had been paid attention to the earth atmosphere harmful. The electrolysis process requires only the electricity and water (H_2O) as a raw materials to generate the H_2. In the electrolysis process, the H_2O was spitted into H_2 and O_2 by supplied the electricity. This method has the advantage than the steam reforming process because of none of polluted gas is emitted [9,10]. However, the energy to be applied for the H_2O to split is rather much and expensive. A few passes decade, the photoelectrochemical (PEC) water splitting by the photocatalytic process has become an interested topic research [11], because this process can be also splitting the H_2O into the H_2 and O_2 similar to the electrolysis process with less energy requirement [12].

The PEC is composed of two electrodes, which were fabricated by the p-type or n-type semiconductor materials and/or metal or both of semiconductors. The p-type semiconductor materials have advantage than the n-type since, almost of p-type semiconductor materials has a low energy bandgap. The p-type semiconductor that have been applied in the PEC are, e.g. copper oxide [13,14], copper bismuth oxide [15-16], spinel copper ferrite oxide [17,18] and chromium oxide [19] and etc. [20-25] Copper oxide has many morphologies and form with depended on the synthesis process. The energy bandgap of copper oxide is typical 1.5-2.0 eV varied on phase and on their nanostructures [26-28].

Previous work showed that the CuO and Cu_2O were well applied as the photocathode material used in the PEC. As many comparisons on the performance [29], the CuO has more benefit on the solar light harvesting conversion energy as the Cu_2O due to the low bandgap. However, in some report showed that the Cu_2O has better performance that the CuO due to the well crystallinity and charge transport in the lattice. One of the obstacles to utilize the Cu_2O is that

* Corresponding author: asanee.s@sciee.kmutnb.ac.th
https://doi.org/10.15251/DJNB.2024.192.901

of the high electron-hole recombination rate. The charge carrier recombination rate can be improved by doping or applied the heterostructure to other materials.

In this research, the Cu_2O nanorod and $Cu_2O/ZnFe_2O_4$ p-n heterostructure photocathodes were studied. The materials were synthesized by electrochemical deposition method. The materials have been characterized by X-ray diffraction and the surface morphology was studied by scanning electron microscopy. The energy bandgap of materials was studied by UV–vis diffuse reflectance spectroscopy. The electrochemical properties of the photoelectrode were studied by various techniques, such as chopped light voltammetry and electrochemical impedance spectroscopy. Finally, the results were also discussed.

2. Experiment

2.1. Sample preparations

First, a fluorine-doped tin oxide glass slide (FTO) was cut into 1.0 cm × 2.0 cm. The FTO was cleaned with acetone, ethanal, and deionized water (DI water) ultrasonically for 10 min for each step. The Cu_2O and $Cu_2O/ZnFe_2O_4$ nanorods grow on an FTO substrate by electrochemical deposition. In this synthesis, the two electrodes were used where the current and voltage were fixed to 5 $mA.cm^{-2}$ and -0.4 V, respectively. For the case of Cu_2O synthesis, the $CuNO_3$ of 5 mmole was dissolved in 50 mL DI. The Cu precursor was stirred for 10 min. The bare FTO was connected to the negative of the electrical power supply while the positive pole was connected to the Pt wire. Then, the electrical power supply was turned on for 10 min. At this process, the black thin film of the pristine Cu was coated on the FTO. It was transferred to the 1 M NaOH, then ultrasonicated for 10 sec, and submerged for 50 sec. The greenish film was obtained.

For $ZnFe_2O_4$ coating on Cu_2O process, the 5 mmol of $FeNO_3$ and 2.5 mmol of $ZnNO_3$ were dissolved in 50 mL DI water. The as-prepared Cu_2O nanorod was connected to the negative pole of the power supply, while the Pt wire was connected to the positive pole of the power supply, similar to the previous section. In this process, the times of synthesis was difference, which were 5, 10 and 15 min. Hence, the samples were lebeled as pure, 5CZFO, 10CZFO and 15CZFO corresponding to the pure Cu_2O, 5 min $Cu_2O/ZnFe_2O_4$, 10 min $Cu_2O/ZnFe_2O_4$ and 15 min $Cu_2O/ZnFe_2O_4$, respectively. Finally, all product was annealed at 500 °C in air for 2 hr, except the Cu2O.

2.2. Characterizations

The Structure of samples was studied by X-ray diffraction (XRD, Bruker D8 eco) with Cu-Kα radiation). Scanning Electron Microscopy (SEM, JEO JSM-6700F) characterized surface morphology, microstructure, and interface. The chemical species of sample was analyzed by X-ray photoelectron spectroscopy. The optical absorption of materials was studied by UV-Vis Spectrophotometer (Shimadzu UV-2600). All electrochemical test was performed by electrochemical work station (Zahner electrik).

2.3. Photoelectrochemical performances

The three-electrode method was used to study the photoelectrochemical performance. The photocathode was set as the working electrode, the Pt wire was set as the counter electrode and the Ag/AgCl was set as the reference electrode. In our study, 0.5 M NaOH was used as an electrolyte. In the chopped light voltammetry study, the samples were scanned from -0.5 to +0.5 V (vs. Ag/AgCl). Therefore, the type of material can be examined. During the scan, the light was chopped on and off, where the light intensity was set to 100 $mW.cm^{-2}$. Thus, the photocurrent generated according to the process is due to the semiconductor's corresponding electron and hole separation. The amount of photocurrent refers to the H_2 and O_2 generated by the PEC. Electrochemical Impedance Spectroscopy (EIS) was tested at a fixed -0.4 V of the applied bias voltage. In the Mott-Schottky analysis, in this case, a 1 kHz fixed frequency was applied, and the applied voltage was scanned from +0.2 to 1.7 V (vs. Ag/AgCl) under dark illumination.

3. Results and discussion

Fig.1 shows the XRD patterns of the bare FTO substrate, Cu_2O coated on FTO substrate and $Cu_2O/ZnFe_2O_4$ (15CZFO) coated on FTO substrate. The diffraction pattern of FTO was matched well to the JCPDS 46-1088 [30]. After Cu_2O was deposited, the diffraction peak of Cu_2O was found which was matched to cuprite structure (JCPDS# 74-1230) [31]. There is only a peak located at 37° which was corresponded to the (111) miller plane. The heterostructure of $Cu_2O/ZnFe_2O_4$ coated on FTO showed the main peak locate at 19° and 30.5°. These diffraction peaks were matched to the $ZnFe_2O_4$ structure (JCPDS# 22-1012) [32]. Therefore, their diffraction peaks were corresponding to the (111) and (220) plane of $ZnFe_2O_4$.

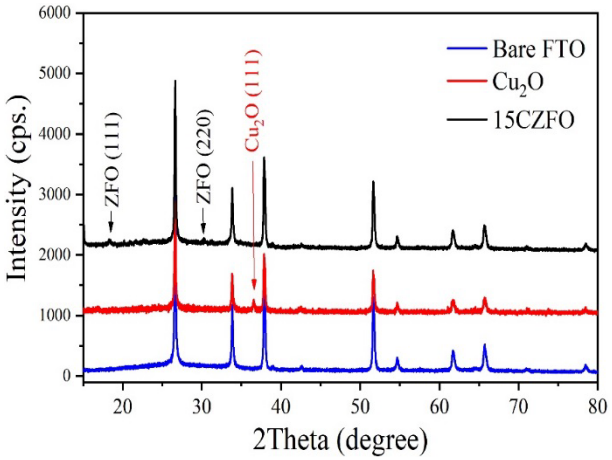

Fig. 1. XRD patterns of bare FTO, Cu_2O and 15CZFO thin films.

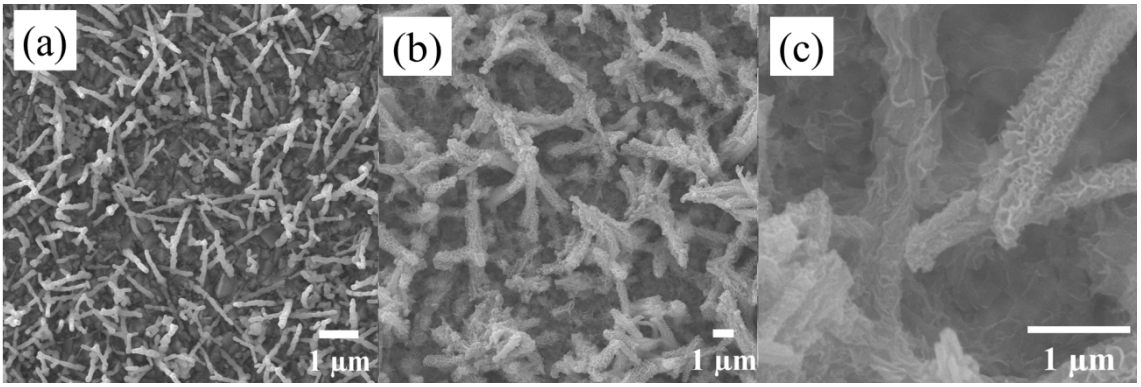

Fig. 2. Top-view SEM images of (a) Cu_2O nanorod, (b) $Cu_2O/ZnFe_2O_4$ and (c) enlarged imaged of $Cu_2O/ZnFe_2O_4$.

The microstructure and surface of all nanostructure coated on FTO substrate were showed in Fig. 2. In Fig. 2a, the Cu_2O nanorod was inclined to the substrate. Compared between the Cu_2O and $Cu_2O/ZnFe_2O_4$ as showed in Fig. 2a and Fig. 2b, one can be observed that the Cu_2O rod was enveloped by the $ZnFe_2O_4$ material. Furthermore, the clear $Cu_2O/ZnFe_2O_4$ heterostructure was illustrated in Fig. 2c.

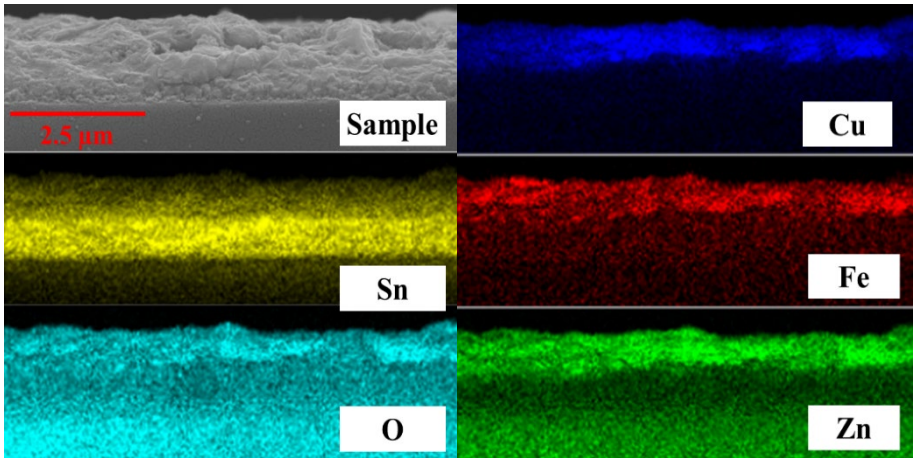

Fig. 3. Cross section of SEM and EDS mapping of $Cu_2O/ZnFe_2O_4$ coated on the FTO substrate.

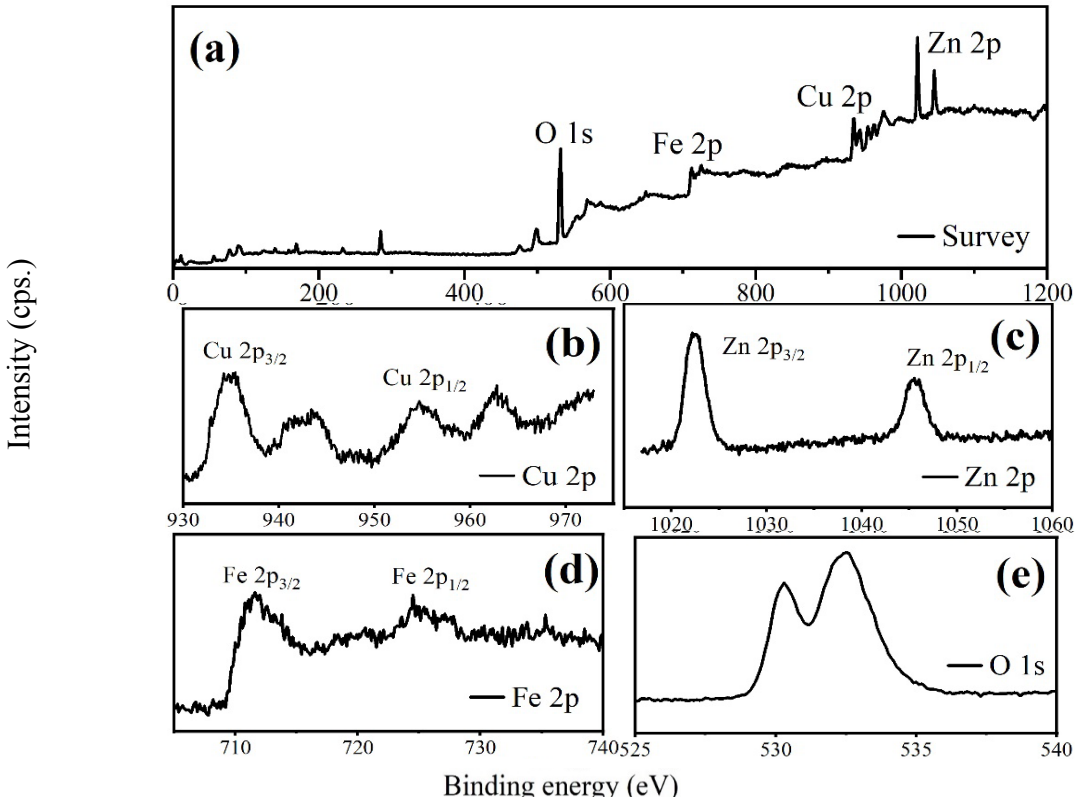

Fig. 4. (a) survey XPS spectrum of $Cu_2O/ZnFe_2O_4$ (15CZFO) sample, (b) Cu 2p, (c) Zn 2p, (d) Fe 2p and (e) O 1s atomic energy.

Fig. 3 showed the cross-section of the film. According to the SEM image, the film thickness was about 2 µm. The energy dispersive showed all element were found on the FTO substrate, which were SnO (FTO), Cu, Fe, Zn and O atoms. It was noticed that the Cu_2O and $ZnFe_2O_4$ were mixed well through the FTO substrate.

Fig. 4 showed the XPS analyst of $Cu_2O/ZnFe_2O_4$ sample. Fig. 4a showed the survey energy spectrum of $Cu_2O/ZnFe_2O_4$ thin film that found all elements presented in the film according to the electrochemical deposition and annealing process. The peak positions were calibrated by the C 1s which wildly used as a standard reference. Fig. 4b showed the Cu 2p1/2 and Cu 2p3/2 spectrum. Fig. 4c illustrate the Zn 2p which comprised of Zn 2p1/2 located at 1045 eV

and Zn 2P 3/2 located 1022 eV. Fig. 4d showed the Fe 2p and Fig. 4e showed the O 1s spectra. Such these present of each element species confirmed the coexistence of Cu_2O and $ZnFe_2O_4$ on the FTO substrate.

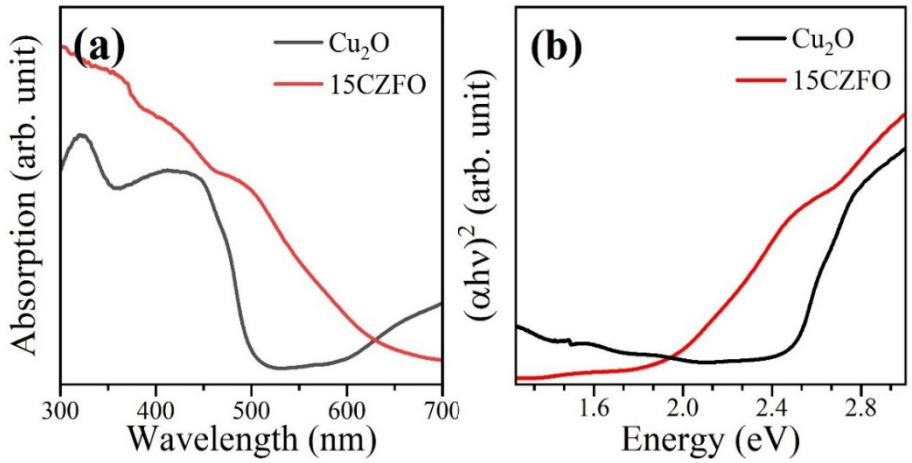

Fig. 5. UV-visible and Tauc plot.

The Tauc plot was used to estimate the energy gap of material where the equation is expressed as followed,

$$\alpha h\nu = A\left(h\nu - E_g\right)^n \tag{1}$$

where, α is the optical absorption coefficient, A is the characteristic constant, ν is incident photon frequency, h is Planck's constant and n is a power factor. In this work, the value of n is set to 1/2 which is suitable to the direct transition of Cu_2O and $Cu_2O/ZnFe_2O_4$ heterostructure materials [33]. Plotting $(\alpha h\nu)^2$ against the photon energy $(h\nu)$ can extract the linear part on the energy axis to get the bandgap of the sample. The absorption and the Tauc plot were showed in Fig. 5. Fig. 5a showed the UV-visible absorption of Cu_2O and $Cu_2O/ZnFe_2O_4$ (15CZFO) and their estimated energy bandgap as shown in Fig. 5b. The Tauc plot yield the bandgap of Cu_2O equal to 2.4 eV and the 15CZFO equaled to 1.8 eV, respectively. As a result, the $ZnFe_2O_4$ coated reduced the bandgap of main Cu_2O by 0.6 eV. Thus, this evidence may imply the better performance in solar energy harvesting of $Cu_2O/ZnFe_2O_4$ over the pure Cu_2O.

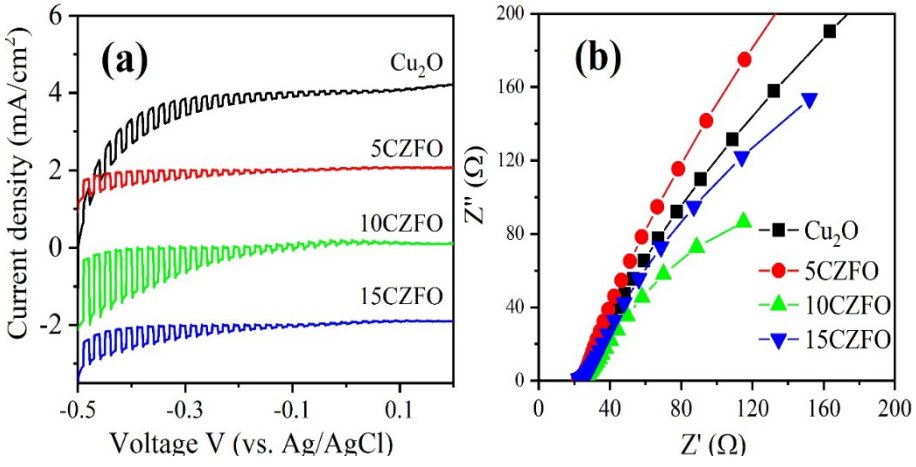

Fig. 6. Linear swept voltammetry and Nyquist plots of as-prepared Cu_2O, 5CZFO, 10CZFO and 15 CZFO photocathode.

The performance of all photocathode was investigated by CLV method. In this CLV experiment, the voltage applied across the working electrode and counter electrode was varied to identified the type of the photoelectrode. As a result showed in Fig. 6a, upon the light turn on and off, the semiconductor was active at the negative regime which allowed us to know the type of this semiconductor. All Cu_2O and $Cu_2O/ZnFe_2O_4$ photoelectrode exhibited the p-type characteristic. The photocurrent density of CLV experiment reflected the performance of the photoelectrode. Therefore, the highest photocurrent density was 10CZFO which was around 2 $mA.cm^{-2}$ at -0.5 V (vs. Ag/AgCl) applied bias voltage, which is greater than the Cu_2O around 2 times.

Furthermore, the Fig. 6 studied the EIS of the PEC under applied bias of -0.4 V (vs Ag/AgCl) and white light irradiation. The impedance of the photocathode can be compared by the Nyquist plot. The small arc radius of Nyquist plot suggests the PEC has low internal impedance and vice versa. Hence, the arc of 10CZFO exhibited the smallest radius, which was signified that it had a low charge transfer resistance comparing the other photocathodes.

4. Conclusions

In this study, the pure Cu_2O and $Cu_2O/ZnFe_2O_4$ photoelectrodes were studied for the PEC device. The photoelectrode was fabricated by the electrochemical deposition method and heat treatment method. The structural and chemical structure of thin film were characterized by XRD, SEM and XPS method which was clearly confirmed their phase of these materials. The electrochemical test showed that all photoelectrode exhibited the p-type characteristic photocathode. The photocurrent density of Cu_2O was 1.0 $mA.cm^{-2}$ while the 15CZFO was 2.0 $mA.cm^{-2}$ at -0.5 V (vs. Ag/AgCl) applied bias voltage. As a result, the heterostructure $Cu_2O/ZnFe_2O_4$ showed the advances in the high photocurrent density than the pure Cu_2O. The improvement of photocurrent was due to the smaller bandgap and the lower internal resistance as evidence from UV-DSR and EIS analysis.

Acknowledgements

This study was funded by King Mongkut's University of Technology North Bangkok (contract no. KMUTNB-66-KNOW-06).

References

[1] Z. Rubab, P. Erum, Y. Minghui, R. Osama, S. Zubia, A. Maryum, F. Sarah, International Journal of Hydrogen Energy **45**(46), 24518-24543 (2020); https://doi.org/10.1016/j.ijhydene.2020.06.236
[2] H. Ishaq, I. Dincer, C. Crawford, International Journal of Hydrogen Energy **47**(62), 26238-26264 (2022); https://doi.org/10.1016/j.ijhydene.2021.11.149
[3] S. Norazlianie, International Journal of Hydrogen Energy **45**(38), 18753-18771 (2020); https://doi.org/10.1016/j.ijhydene.2020.05.021
[4] M.G. Rasul, M.A Hazrat, M.A. Sattar, M.I. Jahirul, M.J. Shearer, Energy Conversion and Management **272**, 116326 (2022); https://doi.org/10.1016/j.enconman.2022.116326
[5] A. Ganguli, Front Therm Eng **3**, 1143987 (2023); https://doi.org/10.3389/fther.2023.1143987
[6] H. Zhang, Z. Sun, Y. H. Hu, Renewable and Sustainable Energy Reviews **149**, 111330 (2021); https://doi.org/10.1016/j.rser.2021.111330
[7] M. Younas, S. Shafique, A. Hafeez, F. Javed, F. Rehman, Fuel **316**, 123317 (2022); https://doi.org/10.1016/j.fuel.2022.123317
[8] N.A. Burton, R.V. Padilla, A. Rose, H. Habibullah, Renewable and Sustainable Energy Reviews **135**, 110255 (2021); https://doi.org/10.1016/j.rser.2020.110255

[9] M. Katebah, M. Al-Rawashdeh, P. Linke, Cleaner Engineering and Technology **10**, 100552 (2022); https://doi.org/10.1016/j.clet.2022.100552
[10] H. Song, Y. Liu, H. Bian, M. Shen, X. Lin, Energy Conversion and Management **258**, 115513 (2022); https://doi.org/10.1016/j.enconman.2022.115513
[11] Y. Xue, Y. Wang, Z. Pan, K. Sayama, Angewandte Chemie International Edition **60**(19), 10469-10480 (2020); https://doi.org/10.1002/anie.202011215
[12] A. Grimm, W. A. de Jong, G. J. Kramer, International Journal of Hydrogen Energy **45**(43), 22545-22555 (2020); https://doi.org/10.1016/j.ijhydene.2020.06.092
[13] R. S. Moakhar, S. M. H. Hosseinabad, S. M. Panah, A. Seza, M. Jalali, H. F. Arani, F. Dabir, S. Gholipour, Y. Abdi, M. B. Hariri, N. R. Noori, Y. F. Lim, A. Hagfeldt, M. Saliba, Advanced Materials **33**(33), 2007285 (2021); https://doi.org/10.1002/adma.202007285
[14] M. K. Son, L. Pan, M. T. Mayer, A. Hagfeldt, M. Grätzel, J. Luo, ACS Applied Materials and Interfaces **13**(46), 55080–55091 (2021); https://doi.org/10.1021/acsami.1c16590
[15] G. Seo , B. Kim, S. W. Hwang, S. S. Shin, I. S. Cho, Nano Energy **80**, 105568 (2021); https://doi.org/10.1016/j.nanoen.2020.105568
[16] K. Feng, E. M. Akinoglu, F. Bozheyev, L. Guo, M. Jin, X. Wang, G. Zhou, M. J. Naughton, M. Giersig, Journal of Physics D: Applied Physics **53**, 495501 (2020); https://iopscience.iop.org/article/10.1088/1361-6463/abaf25/meta
[17] S. Maitra, S. Pal, T. Maitra, S. Halder, S. Roy, Energy Fuels **35**(17), 14087–14100 (2021); https://doi.org/10.1021/acs.energyfuels.1c02090
[18] R. Tan, Y. J. Jeong, Q. Li, M. Kang, I. S. Cho, Journal of Advanced Ceramics **12**(3), 612-624 (2023); https://doi.org/10.26599/JAC.2023.9220709
[19] F. Bouhjar, L. Derbali, B. Marí, B. Bessaïs, International Journal of Hydrogen Energy **45**(20), 11492-11501 (2020); https://doi.org/10.1016/j.ijhydene.2019.10.215
[20] C. Daulbayev, F. Sultanov, B. Bakbolat, O. Daulbayev, International Journal of Hydrogen Energy **45**(58), 33325-33342 (2020); https://doi.org/10.1016/j.ijhydene.2020.09.101
[21] M. Herbaut, M. Siaj, J. P. Claverie, ACS Applied Nano Materials **4**(2), 907-910 (2021); https://doi.org/10.1021/acsanm.1c00246
[22] M. Mohsin, T. Ishaq, I. A. Bhatti, Maryam, A. Jilani, A. A. Melaibari, N. H. A. Hamdeh, Nanomaterials **13**(3), 546 (2023); https://doi.org/10.3390/nano13030546
[23] S. Aslam, M. Awais, S. Ahmed, M. Safdar, A. A. Buksh, M. Sohail, Journal of Electronic Materials **53**, 1–15 (2024); https://doi.org/10.1007/s11664-023-10794-z
[24] A. R. Fareza, F. A. A. Nugroho, F. F. Abdi, V. Fauzia, Journal of Materials Chemistry A **10**, 8656-8686 (2022); https://doi.org/10.1039/D1TA10203F
[25] W. Wang, M. Xu, X. Xu, W. Zhou, Z. Shao, Angewandte Chemie International Edition **59**(1), 136-152 (2019); https://doi.org/10.1002/anie.201900292
[26] W. J. Lee, X. J. Wang, Coatings **11**(7), 864 (2021); https://doi.org/10.3390/coatings11070864
[27] T. H. Yin, B. J. Liu, Y. W. Lin, Y. S. Li, C. W. Lai, Y. P. Lan, C. Choi, H. C. Chang, Y. Choi, Coating **12**(12), 1839 (2022); https://doi.org/10.3390/coatings12121839
[28] J. Li, X. Jin, R. Li, Y. Zhao, X. Wang, X. Liu, H. Jiao, Applied Catalysis B: Environmental **240**, 1-8 (2019); https://doi.org/10.1016/j.apcatb.2018.08.070
[29] M. Balık, V. Bulut, I. Y. Erdogan, International Journal of Hydrogen Energy **44**(34), 18744-18755 (2019); https://doi.org/10.1016/j.ijhydene.2018.08.159
[30] N. Zhang, D. Dai, P. Hu, S. Guo, H. Yang, ACS Omega **7**(6), 5415–5420 (2022); https://doi.org/10.1021/acsomega.1c06673
[31] X. Zhong, Y. Zhang, Z. Geng, F. Shi, M. Jiang, Y. Sun, X. Wu, K. Huang, S. Feng, Inorganic Chemistry Frontiers **6**, 1660-1666 (2019); https://doi.org/10.1039/C9QI00400A
[32] J. Zhang, J. M. Song, H. L. Niu, C. J. Mao, S. Y. Zhang, Y. H. Shen, Sensors and Actuators B: Chemical **221**, 55-62 (2015); https://doi.org/10.1016/j.snb.2015.06.040
[33] R. Bunea, A. K. Saikumar, K. Sundaram, Materials Sciences and Applications **12**(7), 315-329 (2021); https://www.scirp.org/journal/paperinformation?paperid=110323